Mechanism and Parameters Controlling the Decomposition Kinetics of Na_2SiF_6 Powder to SiF_4

N. SOLTANI, M. I. PECH-CANUL, L. A. GONZÁLEZ, A. BAHRAMI

Centro de Investigación y de Estudios Avanzados del Instituto Politécnico Nacional, Cinvestav-Saltillo. Av. Industria Metalúrgica No. 1062, Parque Industrial Saltillo-Ramos Arizpe, Ramos Arizpe, Coahuila, 25900, México

Received 17 November 2015; revised 22 March 2016; accepted 24 March 2016

DOI 10.1002/kin.20999
Published online 27 April 2016 in Wiley Online Library (wileyonlinelibrary.com).

ABSTRACT: Sodium hexafluorosilicate (Na_2SiF_6) powder has been used as a silicon source for formation of Si_3N_4 coatings by the hybrid precursor system-chemical vapor deposition (HYSY-CVD) route. The quantitative effect of processing time, temperature, gas flow rate, and process atmosphere (N_2 and N_2:5% NH_3) upon the fractional weight loss during the decomposition of Na_2SiF_6 was studied using a standard L_9 Taguchi experimental design and analysis of variance. The decomposition kinetics of Na_2SiF_6(s) was studied theoretically and experimentally in the temperature range of 550–650ºC by applying the shrinking core model. It was found that regardless of atmosphere type, the reaction order is $n \approx 0.12$ and that a two-stage mixed mechanism consisting of chemical reaction and boundary layer gas transfer controls the decomposition rate. The determined fractional weight loss during Na_2SiF_6 decomposition in nitrogen atmosphere is about 1.05–1.5 orders of magnitude greater than that in N_2:NH_3. The gas flow rate affects the dissociation activation energy, being of 121, 109, and 94 kJ/mol in N_2 and of 140, 120, and 115 kJ/mol in N_2:NH_3, for the flow rates of 20, 60, and 100 cm^3/min, respectively, in both atmosphere types. A good agreement is observed by comparing experimental weight loss data with model predictions. © 2016 Wiley Periodicals, Inc. Int J Chem Kinet 48: 379–395, 2016

INTRODUCTION

The wide applications of fluorine compounds entail the need of studying their physicochemical properties and the mechanisms of the chemical processes occurring upon heating. The SiF_4 species have many applications, being the most important one its use as Si source for chemical vapor deposition [1]. Because of the importance of silicon nitride (Si_3N_4) in engineering materials, of its properties and potential applications at high temperature, as well as in microelectronics and optoelectronics, in recent years there has been a growing interest in this material from different perspectives [2,3]. One of the synthesis routes for silicon nitride powders is the chemical vapor deposition technique, using volatile silicon compounds such as $SiCl_4$, SiH_4, SiF_4, or related molecular compounds, which

Correspondence to: Martin I. Pech-Canul; e-mail: martin.pech@cinvestav.mx, martpech@gmail.com.

Supporting Information is available in the online issue at www.wileyonlinelibrary.com.

yield Si_3N_4 powders upon the gas phase reaction with ammonia.

There are five methods for production of silicon tetrafluoride (SiF_4) at a laboratory scale: (a) reaction of elemental silicon with fluorinating agents [4,5] (b) fluorination of silicon dioxide [6,7], (c) fluorination of silicon tetrachloride [8–10] (d) decomposing fluorosilicic acid with concentrated acids [11], and (e) thermal dissociation of metal hexafluorosilicates [12,13]. The obtained SiF_4 by the latter method from Na_2SiF_6 is of high purity, because the solid by-product, sodium fluoride, absorbs impurities. The thermal decomposition of Na_2SiF_6 offers great opportunities to economically synthesize Si_3N_4 as powders, whiskers/fibers, and films/coatings.

Different dissociation mechanisms for Na_2SiF_6 (s) to SiF_4 (g) in different atmospheres with reaction orders from zero to one have been proposed [14–16]. Vanka and Vachuška [14] reported that isothermal decomposition of Na_2SiF_6 powder in dry nitrogen is found to have a reaction order of 2/3, with an activation energy of 182 kJ/mol in the temperature range 341–413°C and is completely different from that reported by Istomin and coworkers [15]. They reported that slow removal of gaseous silicon tetrafluoride from the sample surface was the rate-controlling step, resulting in the observed zero-order reaction kinetics. In tests carried out in Ar atmosphere, Kashiwaya and Cramb assumed a first-order rate equation. The rate constant of dissociation was determined as a function of temperature: $k_c = 87.3 \exp(-12{,}823/T)$, and the activation energy for dissociation was 106.6 kJ/mol in a temperature range from 427 to 1347°C. The gas phase mass transfer did not affect the dissociation reaction [13]. Likewise, from the thermal decomposition of Na_2SiF_6 sphere-shaped specimens in a reactor open to the ambient atmosphere, it was determined an order of reaction of 0.38 and an apparent activation energy of 116.4 ± 1.5 kJ/mol [16].

In a previous work, it has been found that the decomposition reaction of Na_2SiF_6 in nitrogen is of zero order with activation energy of 156 kJ/mol and a rate-determining-step given by the chemical reaction itself [17]. In the present study, a heterogeneous reaction model was developed to represent the solid–gas reaction. When the solid reactant is nonporous, the shrinking particle model and the unreacted shrinking core model are commonly used. For the shrinking particle model, reactions are confined at the surface of the particle. The unreacted shrinking core model is applied when the reactant is converted into another solid material leaving behind the unreacted solid. The converted material, which is sometimes called "ash,"

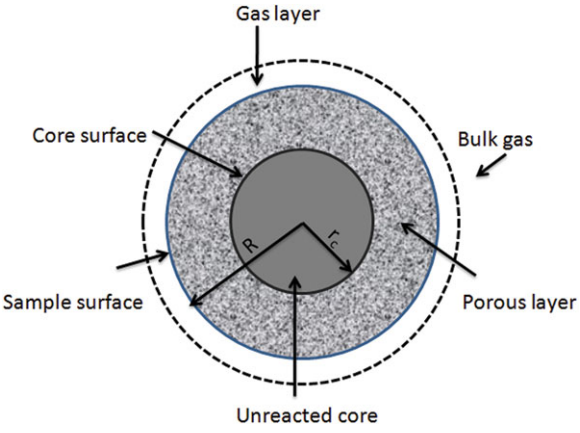

Figure 1 Cross section of a partially dissociated specimen.

is regarded as a porous and inert substance, so that the gas reactants can diffuse from the external surface of the particle to the surface of the unreacted core. Thus, the unreacted core shrinks as the reaction proceeds, but the overall particle size essentially remains constant. Although the unreacted shrinking core model does not precisely represent the whole mechanism of gas–solid reactions, it is accepted as the best simple model for the majority of reacting gas–solid systems [18].

Figure 1 shows a schematic representation of the reaction model presented in this study. For this kind of reaction, the following five steps occurring in succession are visualized: (a) diffusion of reactant from the main body of gas through the gas film to the surface of the solid, (b) penetration and diffusion of reactant through the blanket of ash to the surface of the unreacted core, (c) reaction on the surface between reactant and solid, (d) diffusion of gaseous products through the ash back to the exterior surface of the solid, and (e) diffusion of gaseous products through the gas film back into the main body of the fluid [19].

The final aim of this investigation is coating rice husk ash (derived from rice husk as a potential reinforcement for metal matrix composites) with Si_3N_4 via the chemical vapor infiltration system [20–23]. The synthesis of Si_3N_4 has been conducted at temperature above 1100ºC through the reaction of nitrogen precursor with SiF_4(g) produced during the thermal decomposition of sodium hexafluorosilicate (Na_2SiF_6). The strategic positioning of the Na_2SiF_6 compacts allows controlling the decomposition rate in the temperature range of interest.

Reactions (1)–(3) represent the formation of Si_3N_4 from ammonia, a mixture of nitrogen–ammonia, and nitrogen, respectively, indicating the values of their

corresponding Gibbs free energies.

$$aSiF_{X(g)} + bNH_{3(g)} cSi_3N_4 + dHF_{(g)} + eH_{2(g)} \quad \Delta G_{1300^\circ C} = -843.2\,kJ/mol \tag{1}$$

$$aSiF_{X(g)} + bN_{2(g)} + cNH_{3(g)} dSi_3N_4 + eHF_{(g)} + fH_{2(g)} \quad \Delta G_{1300^\circ C} = -584.6\,kJ/mol \tag{2}$$

$$aSiF_{X(g)} + bN_{2(g)} cSi_3N_4 + dF_{2(g)} \quad \Delta G_{1300^\circ C} = -18.4\,kJ/mol \tag{3}$$

It is clear that thermodynamically it is more feasible to form silicon nitride only in ammonia than in the gas mixture and in the gas mixture than only in nitrogen. This outcome can be explained in terms of the thermal and chemical stabilities of nitrogen and of ammonia. According to the literature, it is more difficult to dissociate nitrogen than ammonia (ionization potential for N_2 and NH_3 are 15.576 and 10.2 eV, respectively) [24].

In addition, the easiness for dissociating NH_3 may be reflected in some extent by the strength of the chemical bonds. At 25°C, the strengths of the H–N and N–N bonds are 75 and 226.8 kcal/mol, respectively [25]. The presence of ammonia in even small amounts is enough for accelerating Si_3N_4 formation. However, silicon nitride films deposited from ammonia show a large number of hydrogen radicals incorporated in their structure. The –SiH radicals formed from the hydrogen atoms incorporated in the network may act as charge traps in the silicon nitride [26,27] and produce a great instability in the electric characteristics of the devices [28].

In spite the various works devoted to study the decomposition of Na_2SiF_6, there are still some discrepancies concerning kinetics, such as the reaction order. It has also been observed that the kinetic parameters are dependent on the decomposition conditions, i.e., temperature, atmosphere, heating rate, gas flow rate, etc. Therefore, new information regarding the influence of gas type and gas flow rate on the dissociation kinetics, and the effect of nitrogen atmosphere on the activation energy for dissociation is still necessary. Moreover, no previous study based on modeling and experimentation has reported an elucidation of the steps that make up the mechanism. Other new contributions of an investigation would be to study the effect of gas flow rate, time and temperature, on the porosity in the NaF ash layer and the influence of the gas flow rate and heating rate on the decomposition temperature. The aim of this investigation was to study the decomposition kinetics of Na_2SiF_6 by systematic variations in processing time, temperature, gas flow rate, and atmosphere (N_2 and N_2-NH_3). The main goal was to propose a decomposition mechanism by considering the shrinking core model. An experimental design (orthogonal array L_9) by the Taguchi method was also used to study the quantitative effect of the processing parameters on the decomposition of Na_2SiF_6 and establish the optimal conditions to attain complete dissociation. Table I shows the standard Taguchi orthogonal (L_9) array used in the investigation.

Table I L_9 Taguchi Experimental Array Used to Study the Effect of Processing Parameters on the Dissociation of Na_2SiF_6

Trial/Run	Temperature (°C)	Time (min)	Gas Flow Rate (cm^3/min)	Precursor (N_2:NH_3)
L1	550	10	20	100:0
L2	550	20	60	5:95
L3	550	40	100	100:0
L4	600	10	20	100:0
L5	600	20	60	100:0
L6	600	40	100	5:95
L7	650	10	20	5:95
L8	650	20	60	100:0
L9	650	40	100	100:0

Note: Heating and cooling rates were 20°C/min and 20°C/min, respectively.

EXPERIMENTAL

Isothermal decomposition tests were performed in a laboratory reactor consisting of a tubular furnace (59300 *Thermolyne*) with an alumina tube (3.1 cm in diameter × 76 cm long) provided with end-cap fittings to control the process atmosphere, gas inlets (and outlets) to supply the nitrogen precursor as well as devices to controlling temperature, gas flow rate, and pressure. The reactor also includes a powder collector and a neutralizer of the gas by-products. The dissociation tests were conducted using 5 g of reactant-grade Na_2SiF_6 (Sigma-Aldrich, Saint Louis, MO, USA) placed in an alumina boat, positioned in the center of the reactor, varying temperature in the range from 550 to 650°C, under N_2 and N_2-NH_3 (5 vol% NH_3 balance N_2) fed at three flow rates (20, 60, 100 cm^3/min). The weight loss was recorded using an electronic balance with a weight accuracy of 0.0001 g. The fractional weight loss (x), from each series of

samples was calculated from the following equation:

$$x = \frac{\text{Weight loss at time } (t)}{\text{Total weight loss after complete decomposition}} \quad (4)$$

The decomposition kinetics of Na_2SiF_6 was investigated by using the shrinking core model, assuming a specimen constant size. The time constant was obtained from curve-fitting toolbox in Matlab software (7.10.0-R2010a). The discrepancy between the data and the estimation model was measured by the sum of squared errors.

Differential thermal and thermogravimetric analyses (DTA/TG) were performed at atmospheric pressure and in a flow of nitrogen using a SDT Q600 (V20.9 build 20) instrument, heating the specimens up to 700°C and maintaining the specimens under isothermal conditions. Three heating rate levels (5, 12.5, and 20ºC/min) and three nitrogen flow rates (20, 60, 100 cm^3/min) were used to determine the variation of peak temperature. The reference material was aluminum oxide. The starting materials and the decomposition products were identified using a Philips 3040 X-ray diffractometer . The X-ray diffraction (XRD) patterns were recorded employing Cu Kα radiation (λ = 1.54 Å) in the 2θ range of 10–80°, using a scan step of 0.03°, a voltage of 40 kV, and a current of 30 mA. The average pore size of reacted Na_2SiF_6 specimens was determined by means of a sorptometer (Quantachrome Autosorb1C, Asic-xtcd6) using the principle of adsorption/desorption of a monolayer of nitrogen on the surface of the solid, based on the methods of Brunauer–Emmett–Teller and micropores analysis.

RESULTS AND DISCUSSION

Differential Thermal Analysis Results for Na_2SiF_6

Figures 2a–2d show the heat flow and weight-loss curves of Na_2SiF_6 decomposition at different heating rates of 5, 12.5, and 20°C/min, respectively, under the nitrogen gas flow rate of 20 cm^3/min. The decomposition of the salt under all three heating rates is found to be starting between 548 and 570°C, where an endothermic peak is observed in all the heating rates tested. As it can be seen from Figs. 2b–2d, with increasing the heating rate from 5 to 20°C/min, the weight of the samples is reduced just in only one step, suggesting that the reaction mechanism, at least with the results obtained within the experimental framework of this work, is not complex. The results of the differential thermal tests of Na_2SiF_6 under various nitrogen flow rates are presented in Table II. As it can be observed, upon increasing the heating rate from 5 to 20°C/min, the initial decomposition temperature augments. On the other hand, it is apparent that the nitrogen gas flow rate does not have any effect on the decomposition (peak) temperature of Na_2SiF_6.

Optimization of Process Parameters

With the aim of determining the percentage of contribution each of the parameters tested to the variability in the conversion fraction of Na_2SiF_6 into gaseous species, an analysis of variance (ANOVA) was performed. The ANOVA (see Table III) showed that the parameter that most significantly affects the decomposition of Na_2SiF_6 is the processing temperature, with a relative contribution of 51% followed by processing time and gas flow rate, with relative contributions of 24% and 15%, respectively. The percentage contribution due to the error term provides an estimate of the adequacy of the experiment. In this case, the magnitude of the error term (7%) suggests that no important factors were omitted in the design of the experiment. Figure 3 depicts the main effects of the controllable factors upon the response variables. According to the main effects analysis, the use of pure nitrogen (Level 1) and the high levels (Level 3) of time, temperature, and gas flow rate enhance the decomposition of sodium hexafluorosilicate and the conversion to gaseous species. Accordingly, the optimum conditions to maximize the decomposition of sodium hexafluorosilicate are as follows: nitrogen precursor as atmosphere, gas flow rate of 100 cm^3/min, processing time of 40 min, and processing temperature of 650ºC.

Isothermal Weight-Loss Measurements

Figures 4 and 5 show the effect of temperature on fractional weight loss as a function of reaction time for two nitrogen precursors under the established gas flow rates. At a fixed reaction time, the conversion increases as temperature increases for any gas flow rate and precursor. At T = 550°C, the reaction rate is too slow to allow a sufficient conversion into gas species in a reasonable reaction time. At fixed temperature, for higher gas flow rates, the conversion fraction increases in a shorter reaction time. By comparing Figs. 4 and 5, it can be seen that the rate of Na_2SiF_6 decomposition under the same condition in the presence of N_2 is about 1.01–1.5 times greater than that in N_2:NH_3. The various slopes of the fractional weight loss as a function of time under different gas flow rates show the possibility of mass transfer control.

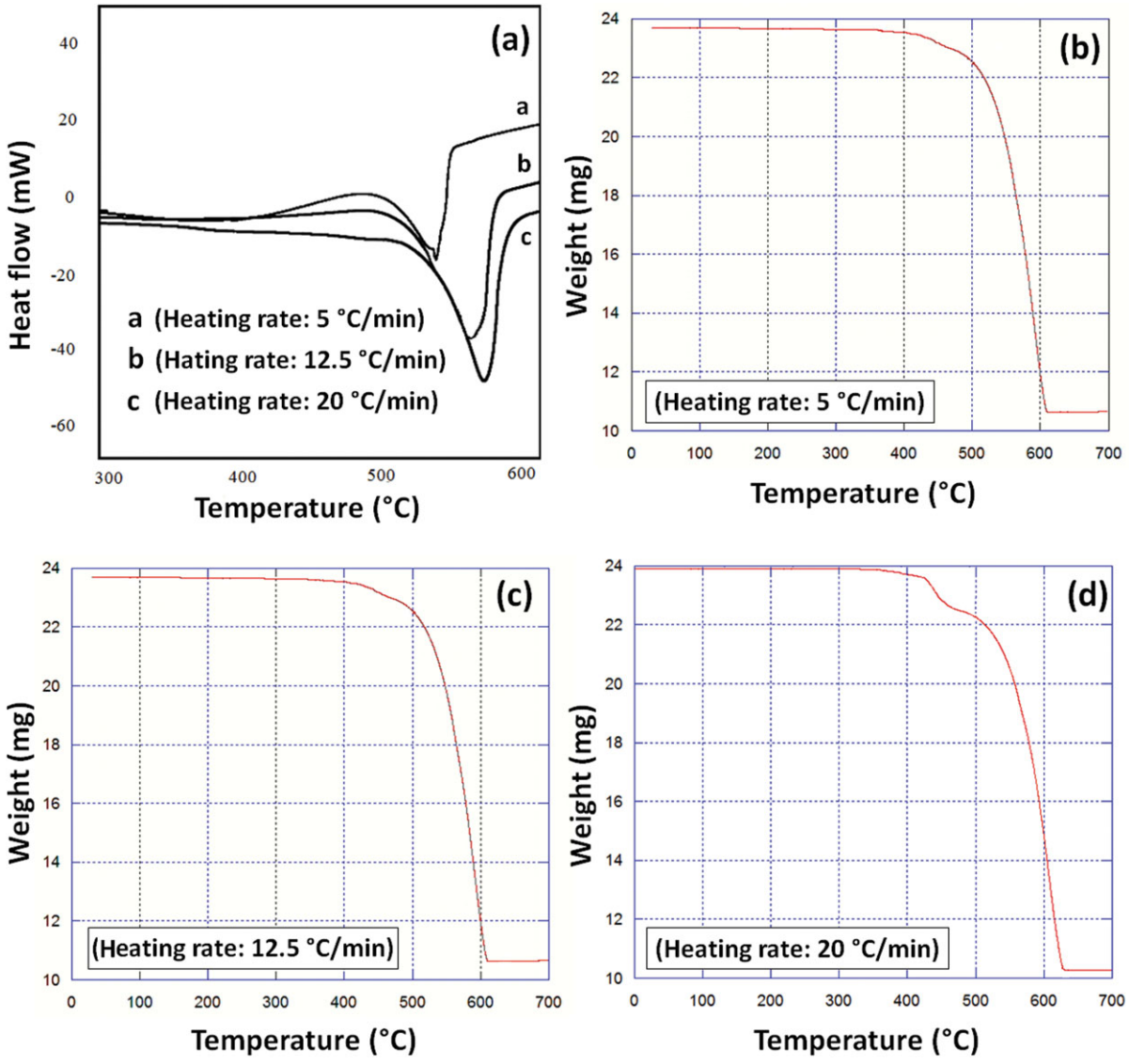

Figure 2 (a) DTA and TG curves of the thermal decomposition of Na_2SiF_6 at heating rates of (b) 5, (c) 12.5, and (d) 20°C/min.

Table II Differential Thermal Analysis Results for Na_2SiF_6

Nitrogen Flow Rate (cm^3/min)	Heating Rate (ºC/min)	T_d [a]
20	5	548
	12.5	566
	20	570
60	5	548
	12.5	565
	20	572
100	5	548
	12.5	565
	20	570

[a] T_d: Decomposition temperature of samples at endothermic peak.

Reactions of the type $A_{(s)} \rightarrow B_{(s)} + C_{(g)}$ can be described by the following equation:

$$\frac{dx}{dt} = kx^n \tag{5}$$

where dx/dt is the dissociation rate of the solid (Na_2SiF_6), x is the fractional weight loss, n is the empirical order of reaction, and k is the rate constant. A series of plots of $\log_{10}$ (reaction rate) versus $\log_{10} x_{SiF_4}$ for a constant heating rate of 20ºC/min and temperatures of 550, 600, and 650ºC under different gas flow rates of N_2 and N_2:NH_3 were constructed. The reaction orders, which were determined using the differential method resulted to be in the range of $n = 0.12$–0.15.

Table III ANOVA Table for Maximizing Conversion Fraction of Na_2SiF_6 into Gaseous Species

Number	Factors	DOF	Sum of Squares	Variance	Contribution Percentage
1	Temperature	2	0.38	0.19	51
2	Time	2	0.11	0.05	15
3	Gas flow rate	2	0.18	0.09	24
4	Type of gas	1	0.022	0.022	3
5	Error	10	0.05	0.005	7

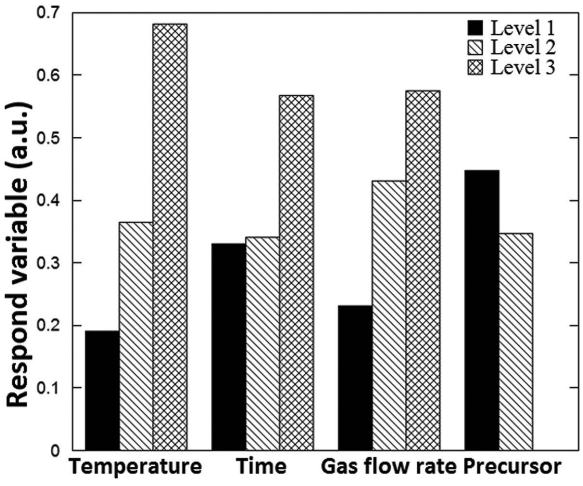

Figure 3 Main effects of the processing parameters (time, temperature, gas flow rate, and precursor) on the conversion fraction of Na_2SiF_6 into gaseous species (response variable).

Plots of $\log_{10}$(reaction rate) versus $\log_{10} x_{SiF_4}$ for different atmospheres, temperatures, and gas flow rates are presented in Figs. 1 and 2 of the Supporting Information. The differential thermal patterns (obtained in DTA/TG tests) also provide a valuable method for estimating the reaction order of a particular reaction. Thus, to confirm the calculated reaction orders, the differential thermal technique—by Kissinger [29]—was used additionally. To quantitatively describe the form of peak, a "shape index (S)" is defined as the absolute value of the ratio of the slopes of tangents to the curve at the inflection points [29]. The determination of this shape index is illustrated in Fig. 6. The reaction order can thus be calculated by the following equation:

$$n = 1.26S^{1/2} \tag{6}$$

Shape index = a/b,
where

$$a = \left(\frac{d^2x}{dt^2}\right)_1$$

$$b = \left(\frac{d^2x}{dt^2}\right)_2$$

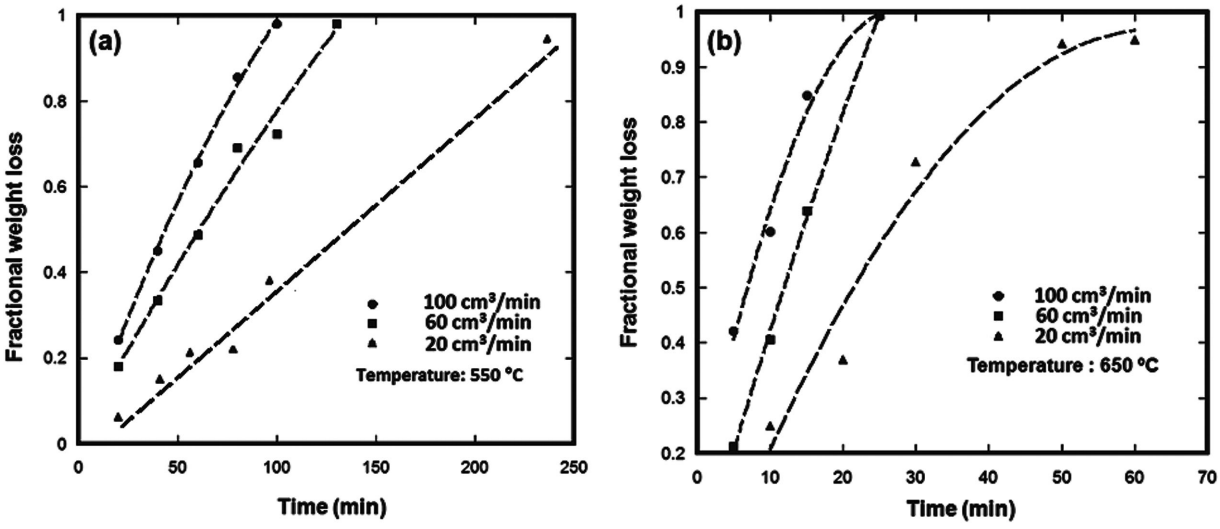

Figure 4 Experimental fractional weight loss measurements versus time at 550 and 650ºC under N_2 atmosphere.

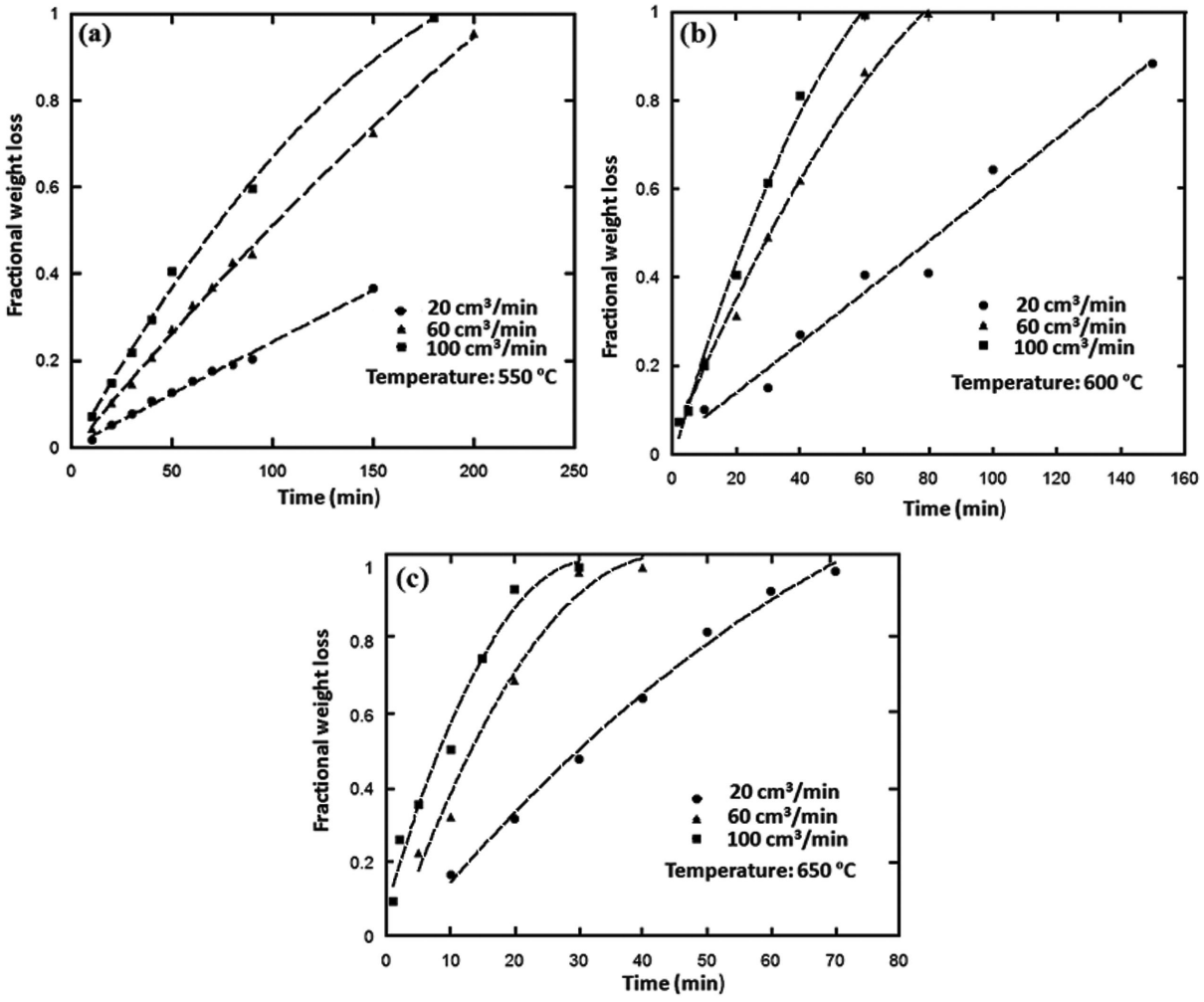

Figure 5 Experimental fractional weight loss measurements versus time at 550, 600, and 650ºC under N_2:NH_3 atmosphere.

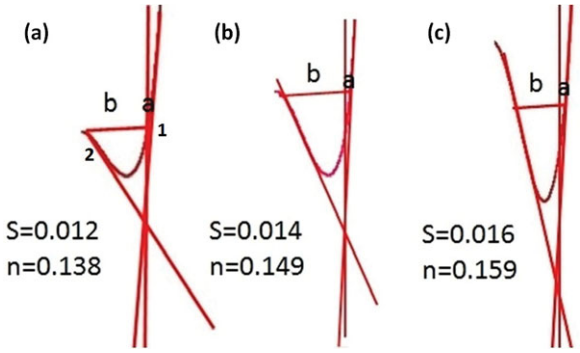

Figure 6 Method for measuring the magnitude of asymmetry in an endothermic differential thermal analysis peak of Na_2SiF_6 decomposition at a heating rate of 20ºC/min for various nitrogen flow rates of (a) 20, (b) 60, and (c) 100 cm^3/min.

It was found that the results of the differential thermal study from DTA/TG tests are in good agreement with those obtained using the differential method. The reaction orders obtained between 0.13 and 0.15. These results show that the different flow rates, temperature, and type of nitrogen precursor do not have any effect on the reaction order and endothermic peak shape.

Representative XRD patterns of specimens after the thermal treatment in constant gas flow rate and time are shown in Fig. 7. The XRD patterns reveal the presence of unreacted Na_2SiF_6 and of cuboid-shaped NaF as the only solid reaction product.

Figure 8a is a representative photomicrograph showing the spherical shape of Na_2SiF_6 powders before the thermal treatment. Figure 8b shows the porous structure of a decomposed Na_2SiF_6 specimen. Microscopic examination by scanning electron microscopy (SEM) complemented with energy-dispersive X-ray

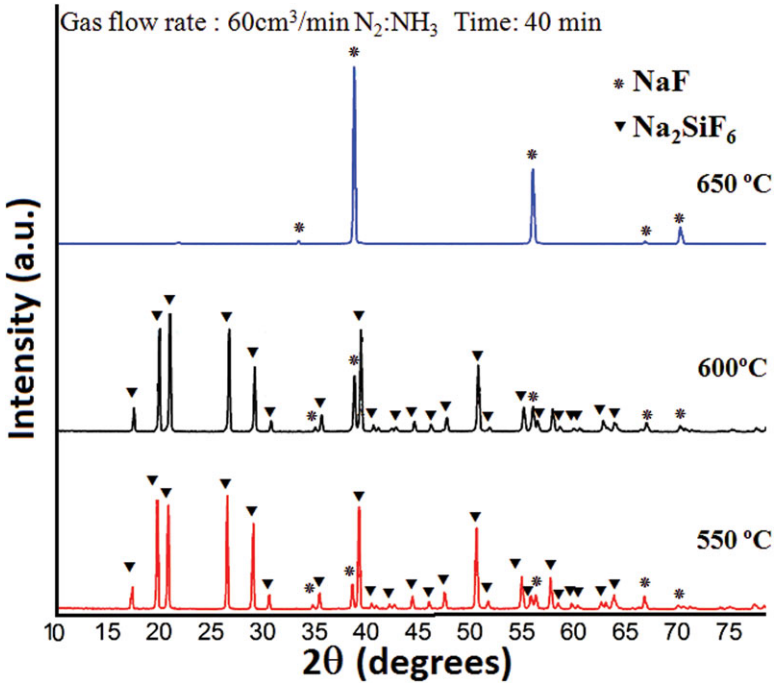

Figure 7 XRD patterns of Na_2SiF_6 decomposed to NaF the thermal treatment.

spectrometry (EDX) analyses showed that the outer surface of partially reacted specimens is NaF. Also, by EDX analysis, it was found that the central core of the powders consists of Na_2SiF_6. These results together support the hypothesis that the dissociation process fits the shrinking core model, in which the core size becomes increasingly smaller and the porous surrounding layer of (NaF) by-product continuously grows as the dissociation reaction proceeds (see Fig. 8c). The backscattered electron signal provided sufficient phase contrast between the sample and the resin, for phase identification and image processing of particle cross sections.

As shown with representative SEM micrographs in Fig. 9, it is apparent that at a constant gas flow rate under the same test time, while the use of low temperatures gives place to specimens with an open structure, treating the specimens at high temperatures produces a finer pore structure.

Reaction and Elucidation of Controlling Mechanism

Since microscopic examination and XRD analyses of partially reacted specimens revealed the presence of two distinct phases, NaF and Na_2SiF_6, the overall reaction was approximated by a single-stage, shrinking core model, based on mass transfer control of the SiF_4 through the reacted shell. The model makes the following assumptions: (1) spherical symmetry, (2) isothermal particle, (3) the reaction is irreversible, and (4) no volume change throughout the reaction. Based on thermodynamic calculations and on previous reports from the literature, the reaction at the spherical surface is given by [12] the following equation:

$$Na_2SiF_{6(s)} \rightarrow NaF_{(s)} + SiF_{4(g)} \tag{7}$$

The overall process can be explained by three operative mechanism steps: surface reaction at the unreacted core surface (che), diffusion of SiF_4 in the ash layer of NaF (dif), mass transfer of SiF_4 through the gas film (external diffusion (ext)). For spherical particles, the analytic relationship between conversion and reaction time depends upon the rate-limiting step. However, it may not be reasonable to consider that one single-step controls the whole process. Neither the chemical reaction and diffusion nor the gas film diffusion mechanism can separately explain all the x–t data. If the process is assumed to be a combination of rate-limiting mechanism such as chemical reaction, diffusion through ash layer, and external mass transfer, the time t to achieve a certain degree of conversion x can be calculated as follows [30]:

$$t = \tau_{che} \times f_{che}(x) + \tau_{dif} \times f_{dif}(x) + \tau_{ext} \times f_{ext}(x) \tag{8}$$

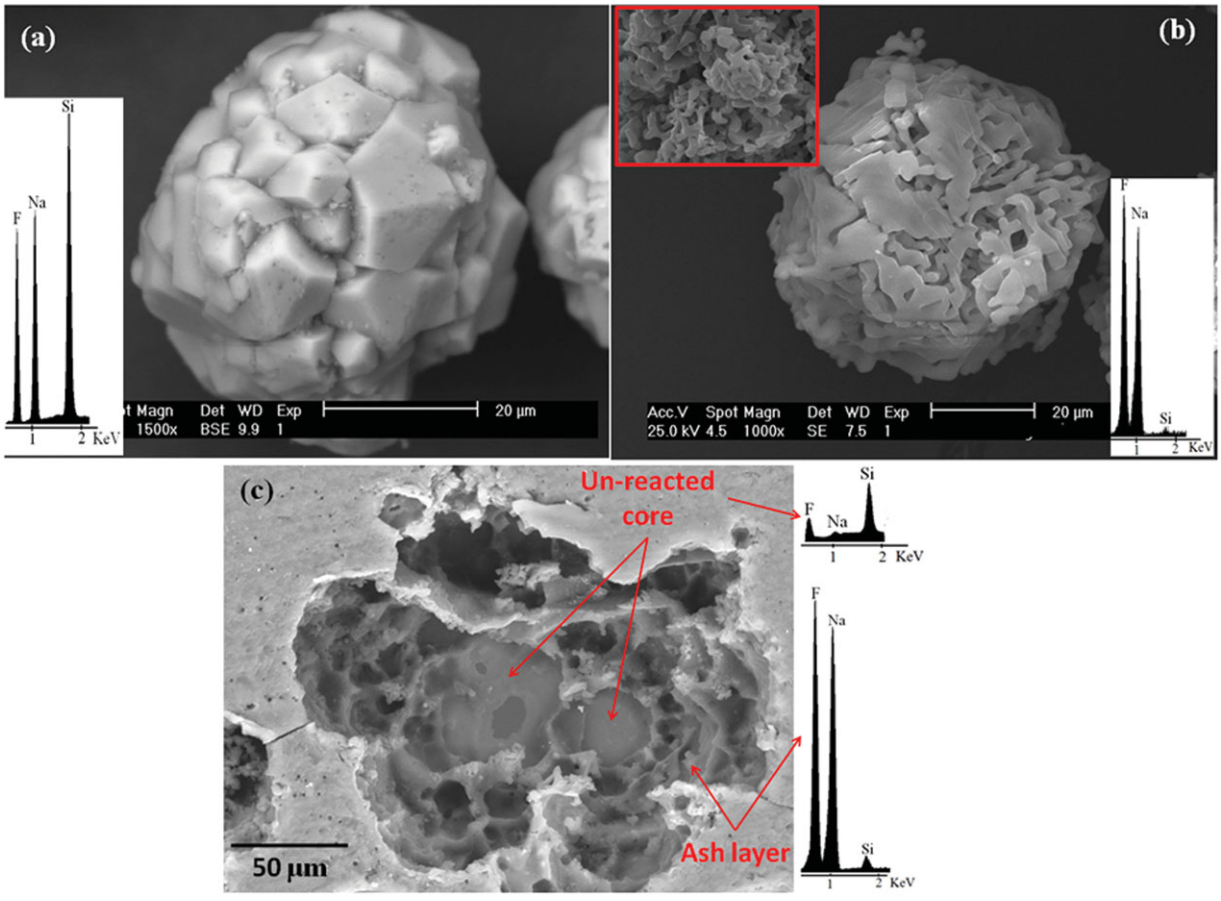

Figure 8 SEM photomicrographs and EDX spectra of the Na_2SiF_6 salt: (a) before and (b) after the thermal treatment (600ºC under N_2:NH_3 flow rate of 60 cm^3/min in 40 min**)** and (c) broken treated particle.

where t is the overall reaction time; τ_{che}, τ_{dif}, and τ_{ext} are time constants; and $f_{che}(x)$, $f_{dif}(x)$, and $f_{ext}(x)$ are conversion functions describing chemical reaction kinetics, diffusion, and mass transfer, respectively, given by [31]:

$$\tau_{ext} = \frac{\rho_c R}{3k_g C_{SiF_4}} \tag{9}$$

$$\tau_{dif} = \frac{\rho_c R^2}{6D_e C_{SiF_4}} \tag{10}$$

$$\tau_{che} = \frac{\rho_c R}{k_s C_{SiF_4}^n} \tag{11}$$

where ρ_c is the molar density of Na_2SiF_6 in a reacting particle, R is the initial radius of the specimen, C_{SiF_4} is the bulk concentration of SiF_4 at the exterior of the specimen, n is the reaction order, k_g is the mass transfer coefficient between the fluid and the particle, D_e is the effective diffusion coefficient of gaseous reactant in the ash layer, and k_s is a rate constant for the surface reaction.

C_{SiF_4} was calculated for the present work by assuming the total pressure of the mixture $P_t = 1$ atm and by using the ideal gas law. P_i, V_i, n_i,X_i, and T are the pressure, volume, number of moles, mole fraction, and temperature of the gas, respectively, and R is the ideal gas constant.

As it can be seen in Figs. 4 and 5, the fractional weight loss during the thermal dissociation of Na_2SiF_6 at constant temperature behaves approximately in a linear way with time; therefore, the concentration of SiF_4 per minute can be considered constant.

$$P_i V_i = n_i RT,\ P_{SiF_4} = C_{SiF_4} RT \tag{12}$$

$$P_t = 1,\ P_{SiF_4} + P_{N_2} + P_{NH_3} = 1$$

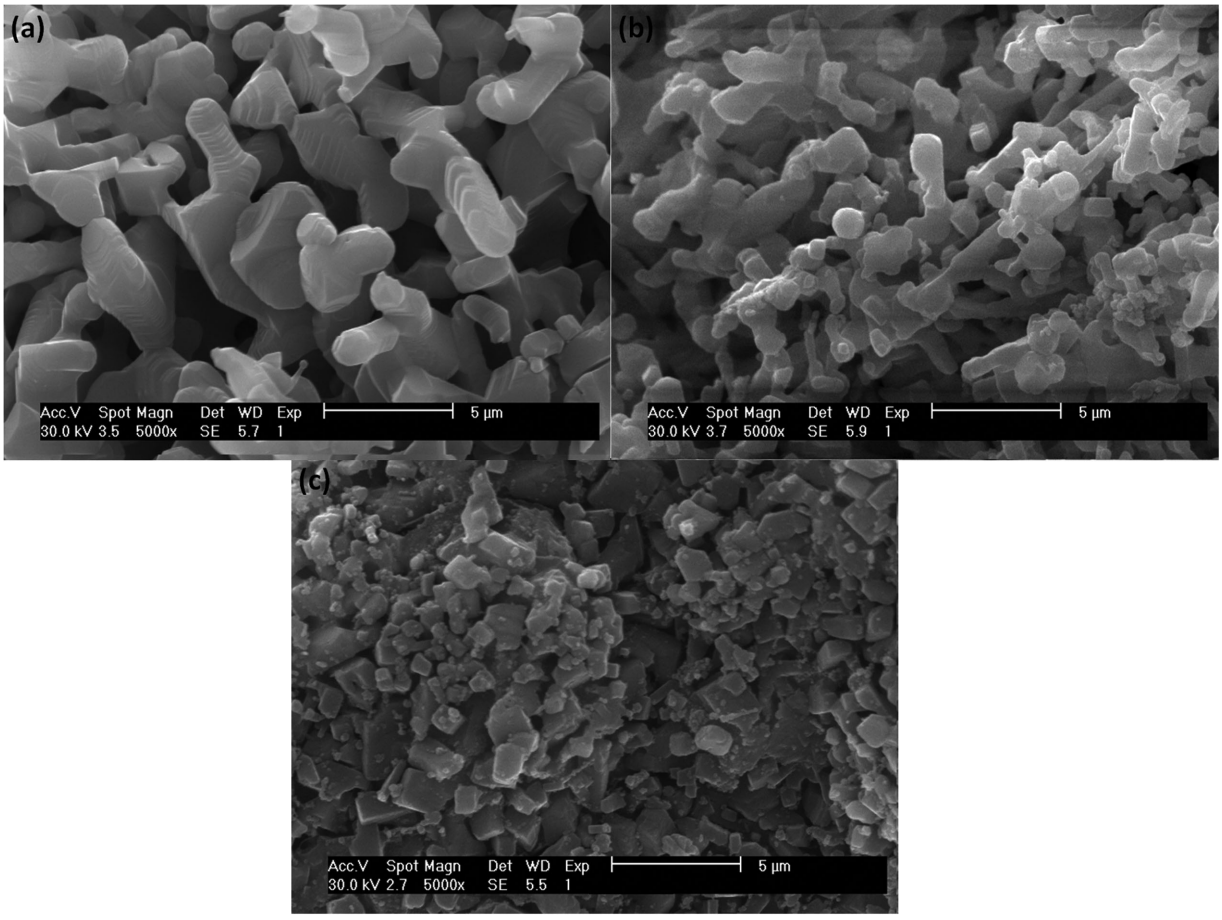

Figure 9 SEM photomicrographs of reacting particle surface at (a) 550, (b) 600, and (c) 650ºC under N_2:NH_3 flow rate of 60 cm^3/min for 40 min.

$$X_{SiF_4} + X_{N_2} + X_{NH_3} = 1$$

$$P_{SiF_4} = X_{SiF_4} \times P_t$$

The conversion functions ($f(x)$) for the different mechanisms are defined as follows [19,30]:

$$\frac{t_{ext}}{\tau_{ext}} = f_{ext}(x) = x \tag{13}$$

$$\frac{t_{che}}{\tau_{che}} = f_{che}(x) = 1 - (1-x)^{1/3} \tag{14}$$

$$\frac{t_{dif}}{\tau_{dif}} = f_{dif}(x) = 1 - 2(1-x) + 3(1-x)^{2/3} \tag{15}$$

To establish the appropriate controlling mechanism of Na_2SiF_6 decomposition, single, double, and triple controlling system, i.e., single mechanism ([$f_{ext}(x)$], [$f_{che}(x)$], [$f_{dif}(x)$]), double mechanism systems ([$f_{ext}(x) - f_{che}(x)$], [$f_{dif}(x) - f_{ext}(x)$], [$f_{che}(x) - f_{dif}(x)$]), and triple mechanism systems ([$f_{ext}(x) - f_{che}(x) - f_{dif}(x)$]) were considered.

Plots of fractional weight loss versus time for all tests were constructed. Constant time and standard deviations from experimental data can be calculated by fitting the plot of time versus fractional weight loss to these equations by considering the single mechanism:

$$t = \tau_{ext} f_{ext}(x);\ t = \tau_{che} f_{che}(x);\ t = \tau_{dif} f_{dif}(x) \tag{16}$$

double mechanism:

$$t = \tau_{ext} f_{ext}(x) + \tau_{che} f_{che}(x);\ t = \tau_{che} f_{che}(x) + \tau_{dif} f_{dif}(x);\ t = \tau_{dif} f_{dif}(x) + \tau_{ext} f_{ext}(x) \tag{17}$$

Table IV Time Constant of Various Mechanisms in One and Multimechanism System under N_2 Stream

N_2 Flow Rate (cm^3/min)	Temperature (ºC)	Time Constant (min)						
		τ_{che}	τ_{dif}	τ_{ext}	$\tau_{dif\ \&\ ext}$	$\tau_{dif\ \&\ che}$	$\tau_{che\ \&\ ext}$	$\tau_{dif\ \&\ ext\ \&\ che}$
20	550	739	2,838	220	955 and 277	734 and 625	226 and 24	–2, 17, and 14
	650	92	88	54	25 and 40	–45 and 138	24 and 50	53, –117, and 25
60	550	276	369	125	50 and 109	–85 and 338	89 and 40	–138, 35, and –10
	650	820	2,960	300	2 and 23	–48 and 84	4 and 23	–15, 22, and 15
100	550	155	144	99	22 and 83	–38 and 295	71 and 40	–6, 51, and 68
	650	31	30	20	16 and 10	–6 and 38	3 and 22	–1, 30, and 2

Table V Sum of Squared Errors for the Different Mechanisms under a Stream of N_2

N_2 Flow Rate (cm^3/min)	Temperature (ºC)	Sum of Squared Errors						
		che	dif	ext	dif & ext	dif & che	che & ext	dif & ext & che
20	550	2,970	3,740	3,740	86	84	4.1	102
	650	2,550	3,080	3,750	108	98	0.5	100
60	550	3,570	4,396	3,410	117	108	0.78	95
	650	4,850	5,700	3,300	46	16	0.1	10
100	550	3,740	5,383	3,100	38	31	2	45
	650	4,060	5,600	4,600	31	25	8.5	40

Table VI Time Constant of Various Mechanisms in Single and Multimechanism System under Stream of NH_3:N_2

N_2:NH_3 Flow Rate (cm^3/min)	Temperature (ºC)	Time Constant (min)						
		τ_{che}	τ_{dif}	τ_{ext}	$\tau_{dif\ \&\ ext}$	$\tau_{dif\ \&\ che}$	$\tau_{che\ \&\ ext}$	$\tau_{dif\ \&\ ext\ \&\ che}$
20	550	157	344	88	56 and 404	–377 and 1,215	250 and 130	146, –409, and 136
	600	329	341	165	29 and 156	–198 and 493	71 and 119	–122, 323, and 54
	650	102	94	65	14 and 56	–102 and 207	24 and 49	–52, 117, and 25
60	550	367	345	203	29 and 189	–268 and 613	151 and 79	224, –399, and 312
	600	108	100	71	27 and 55	–94 and 203	27 and 49	4, –54, and 24
	650	43	39	34	9 and 27	–160 and 106	12 and 25	–51, 90, and 5
100	550	105	217	165	35 and 167	–49 and 251	90 and 87	183, –218, and 192
	600	102	119	49	6 and 52	–75 and 162	14 and 46	–322, 744, and –187
	650	32	31	23	17 and 12	–15 and 47	6 and 22	–1, 23, and 7

and triple mechanism:

$$t = \tau_{dif} f_{dif}(x) + \tau_{ext} f_{ext}(x) + \tau_{che} f_{che}(x) \quad (18)$$

The calculated parameters (Tables IV and VI) and mechanism deviation values (Tables V and VII) obtained by considering single and multimechanisms are shown for both processing atmospheres, N_2 and N_2-NH_3, correspondingly. However, only the best fit curves corresponding to the dominant mechanism are presented. Plots of comparison of the experimental and predicted fractional weight loss for specimens treated in N_2 and N_2-NH_3 under a flow rate of 60 cm^3/min at the different test temperatures are presented in Figs. 10a and 10b.

As it can be observed in Tables IV and VI, both, negative and positive time constants resulted from the calculations. However, since the negative values have no physical meaning, the combination mechanism with positive values and minimal deviations (columns 8 in Tables V and VII) is selected as the one that controls the decomposition kinetics, namely, the combination of chemical reaction and external boundary layer gas transfer.

Table VII Sum of Squared Errors for the Different Mechanisms under a Stream of N_2:NH_3

N_2:NH_3 Flow Rate (cm^3/min)	Temperature (ºC)	Sum of Squared Errors						
		che	dif	ext	dif & ext	dif & che	che & ext	dif & ext & che
20	550	111	210	3,074	86	87	0.14	56.9
	600	3,028	4,447	92	12	297	0.32	297
	650	3,960	5,470	152	17	11.36	7.1	17
60	550	3,674	5,010	128	77	210	0.13	43
	600	4,001	5,504	503	11	76	4.9	13
	650	3,030	5,700	570	42	10	0.38	10
100	550	3,413	5,493	152	71	60	0.15	44
	600	3,602	4,946	540	41	35	2.5	35
	650	3,500	4,704	880	14	47	0.5	9

Although, for all the experimental systems the reaction is controlled by both chemical reaction and gas layer diffusion, the value of external boundary layer gas transfer resistance to chemical reaction resistance ratio ($\frac{\tau_{ext}}{\tau_{che}}$) suggests that decomposition of Na_2SiF_6 is mostly governed by reaction at low temperatures ($\frac{\tau_{ext}}{\tau_{che}} < 1$) and by external boundary layer gas transfer at high temperatures ($\frac{\tau_{ext}}{\tau_{che}} > 1$). In addition, the value of $\frac{\tau_{ext}}{\tau_{che}}$ shows that by increasing temperature, the proportion of gas layer diffusion is larger for higher flow rates, and the impact of this phenomenon is stronger under nitrogen stream. This value at $T = 650$°C can be changed by increasing the gas flow rate from 1 to 4 (right-hand vertical axis) for N_2:NH_3 and from 2 to 7 for N_2 precursor. The values of k_s and k_g were calculated by Eqs. (6) and (8), respectively. The influences of temperature and gas flow rate on the rate constant and mass transfer coefficient are summarized in Tables VIII and IX.

Figure 11 shows that the value of $\frac{k_g}{k_s}$ ratio decreases by increasing temperature. As discussed before, the increase in temperature results in increment of equilibrium conversions. This behavior is essentially attributed to a higher rate constant and to the acceleration of the gas transfer process through the boundary layer at higher temperature. In addition, it should be mentioned that both values of k_s and k_g augment by increasing the gas flow rate for both N_2 and N_2:NH_3 system, but k_s and k_g show the highest values under stream of nitrogen. An increase in the gas velocity causes a reduction in the boundary layer thickness [32], and, consequently, a change in the mass transfer coefficient and a rapid removal of gaseous silicon tetrafluoride from the sample surface can be expected as a result a higher decomposition rate of the salt.

The diffusion mechanism does not appear to have any effect on the decomposition rate of Na_2SiF_6. The highest sum of squared errors (see Tables V and VII) attributed to the pore diffusion process in the best fitted plot between the experimental and calculated data suggests that the diffusion step should be too fast as to be considered the controlling stage. The effect of time, temperature, flow rate, and nitrogen precursor on the average pore diameter was investigated (Fig. 12). At a fixed reaction time, the average pore size decreases as temperature increases regardless of the gas flow rate. This can be visualized in specimens treated in N_2:NH_3, where it was observed that at $t =$ 10 min the pore size is larger than at $t = 30$ min. A possible explanation to this observation is by the partial sintering of $NaF_{(s)}$ by-product—which occurs between 640 and 926°C [33]—similarly to that observed in the calcination of limestone ($CaCO_3$), which decomposes into ($CaO_{(s)}$) and $CO_{2(g)}$ [34]. With an increase in temperature and time, CaO sintering occurs, manifested by a reduction in pore size [35]. In addition, for specimens treated in N_2:NH_3, at a fixed temperature, with an increase in the gas flow rates the pore size decreases. This can be explained in terms of the Kozeny–Carman equation, which inversely relates the specific surface area of a material in a porous bed with the flow rate through a porous media [36,37].

In this specific case, N_2 or N_2:NH_3 pass through the NaF ash layer (the porous medium). It should be pointed out that because of the likeness in the viscosities of N_2 and of N_2: 5% NH_3, similar results were observed in tests conducted under a stream of nitrogen [38].

In light of the previous discussion, it can be concluded that regardless of the pore size in the NaF ash layer, the decomposition process will take place completely, and thus the diffusion process does not appear to be the controlling stage.

As the decomposition reaction is a thermally activated process, the activation energy was determined

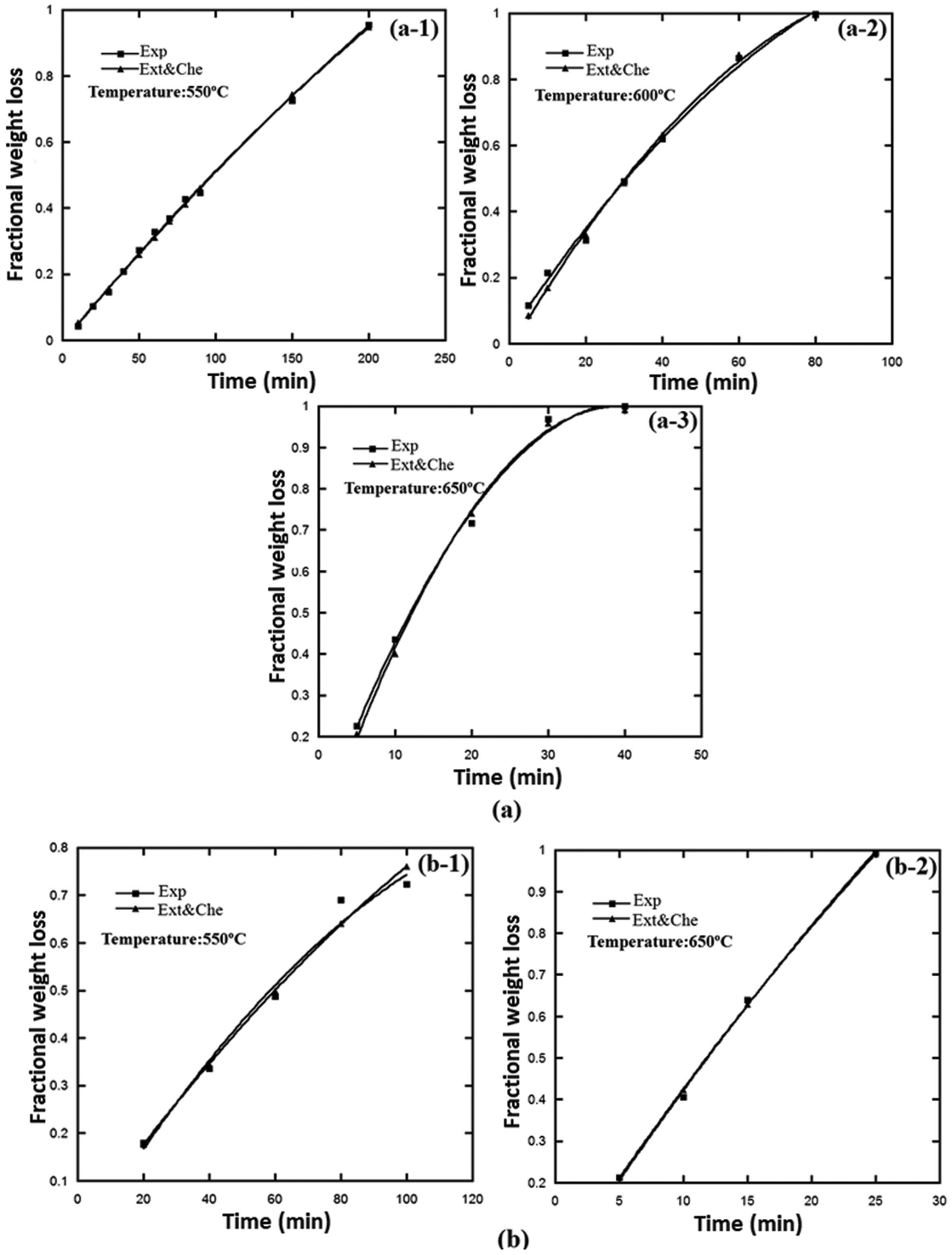

Figure 10 Comparison of the experimental and predicted results of double mechanism (ext & che) for samples under stream of (a) N_2:NH_3 and (b) N_2 with flow rate of 60 cm^3/min.

using Arrhenius' equation. While for the tests in N_2:NH_3, the activation energies for formation of the gaseous species from Na_2SiF_6 are 140, 120, and 115 kJ/mol, in N_2 the values of E_a are 121, 109, and 94 kJ/mol for flow rates of 20, 60, and 100 cm^3/min, respectively. It is thus clear that atmosphere plays an important role in the decomposition kinetics of Na_2SiF_6 and that interestingly, in N_2, a lower activation energy

Table VIII Calculated Effective Parameters of Na_2SiF_6 Decomposition under N_2 Stream

N_2 Flow Rate (cm^3/min)	Temperature (°C)	k_s (m/min)	k_g (m/min)	E_a(kJ/mol)
20	550	9.4×10^{-7}	2.01×10^{-7}	121
	650	7.2×10^{-6}	4.77×10^{-6}	
60	550	1.8×10^{-6}	2.44×10^{-7}	101
	650	3.46×10^{-5}	1.14×10^{-6}	
100	550	2.89×10^{-6}	3.39×10^{-7}	94
	650	5.9×10^{-5}	1.74×10^{-6}	

Table IX Calculated Effective Parameters of Na_2SiF_6 Decomposition under N_2:NH_3 Stream

N_2:NH_3 Flow Rate (cm^3/min)	Temperature (°C)	k_s (m/min)	k_g (m/min)	E_a (kJ/mol)
20	550	7.1×10^{-7}	1.01×10^{-7}	140
	600	2.49×10^{-6}	2.6×10^{-7}	
	650	7×10^{-6}	4.12×10^{-7}	
60	550	1.3×10^{-6}	1.25×10^{-7}	120
	600	6.74×10^{-6}	8.62×10^{-7}	
	650	1.07×10^{-5}	9.7×10^{-7}	
100	550	2.1×10^{-6}	1.34×10^{-7}	115
	600	1.3×10^{-5}	1.32×10^{-6}	
	650	2.9×10^{-5}	1.1×10^{-6}	

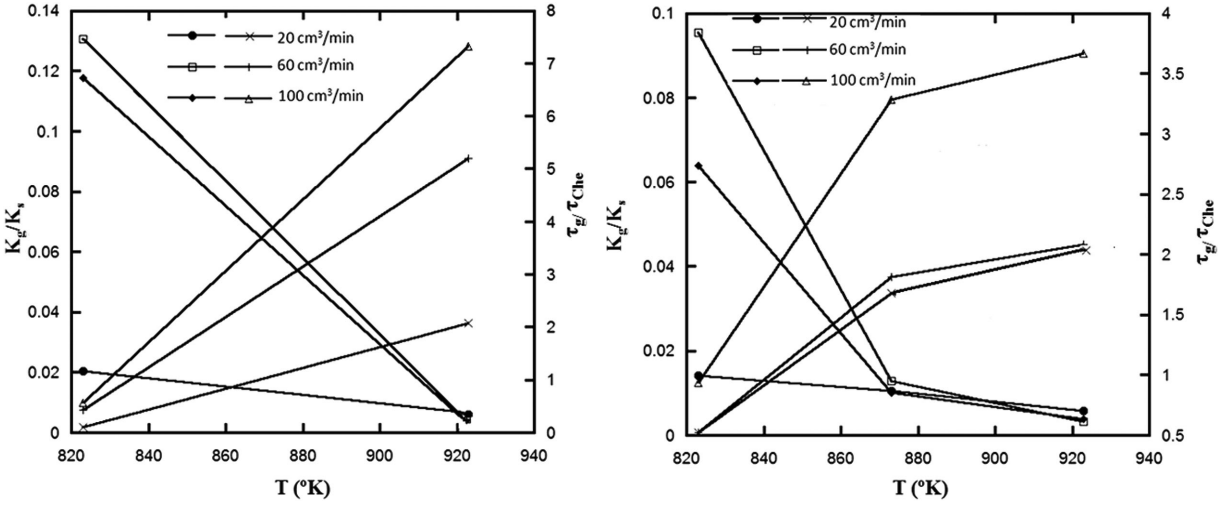

Figure 11 k_g/k_s and τ_g/τ_s versus T under various feeding flow rates of (a) N_2 and (b) N_2:NH_3.

is required than in N_2:NH_3 (see Fig. 13). However, the activation energy values reported for an open reactor to the atmosphere and a reactor operating in argon are 116 and 106 kJ/mol, respectively [1,2], which are lower but comparable to those obtained with the lowest nitrogen flow rate (20 cm^3/min) used in this study. Vanka and Vachuška [14] proposed a two-stage mechanism for the decomposition reaction and reported an activation energy of 182 kJ/mol under dry nitrogen in closed-system DTA measurements. The differences between the reported values and the activation energy determined in the current study clearly show the influence of test conditions and the need for determination of E_a values which stand for a variety of applications.

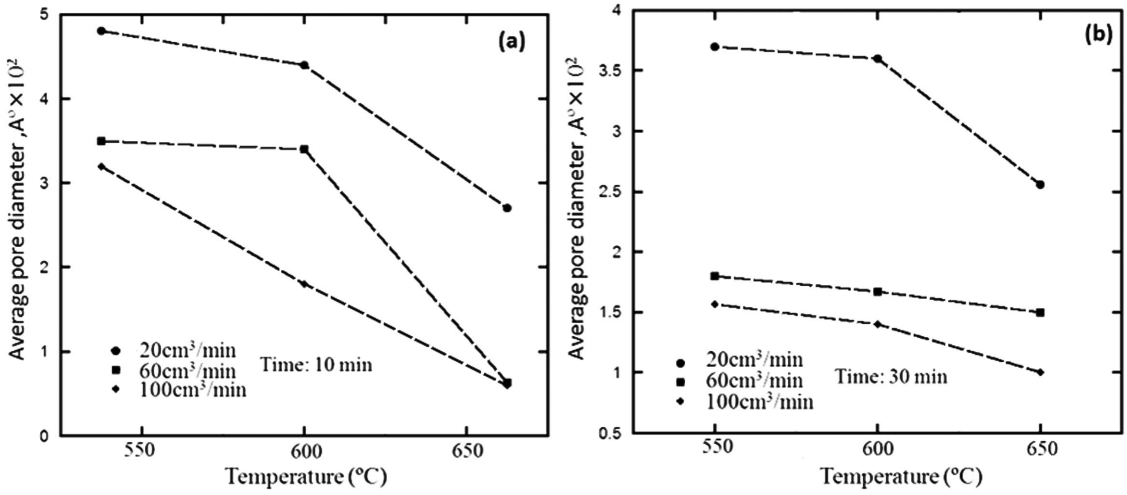

Figure 12 Influence of the gas flow rate on average pore diameters as a function of temperature for (a) 10 min and (b) 30 min, under N_2:NH_3 stream.

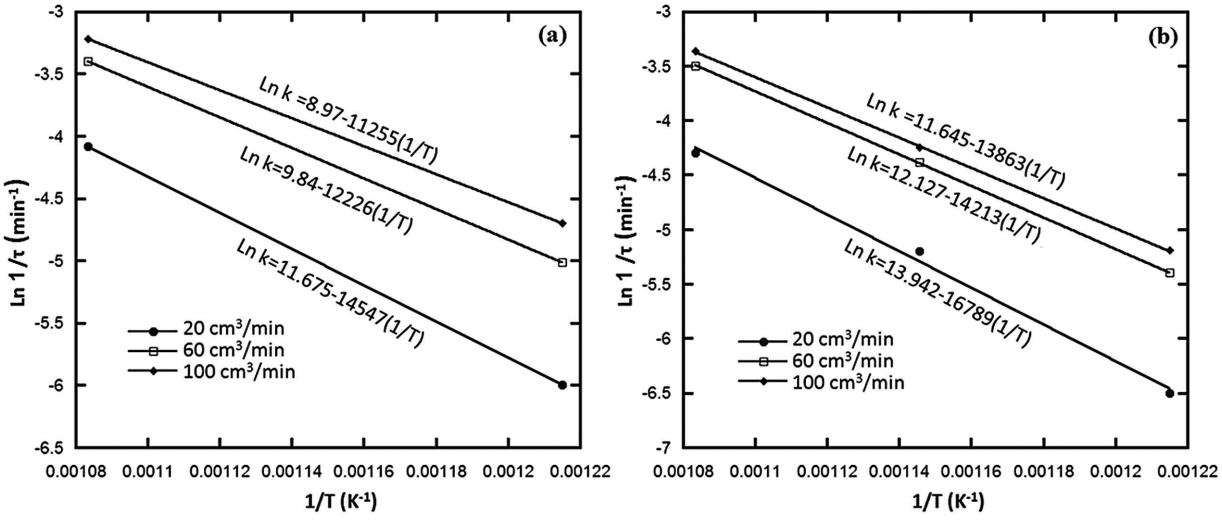

Figure 13 Arrhenius plot ($1/\tau$ vs. $1/T$) for the decomposition reaction under various flow rates of (a) N_2 and (b) N_2:NH_3.

CONCLUSIONS

Based on the previous results and discussion, within the framework of the experimental design—in the range of parameters and levels established for this study—it can be concluded that

- Decomposition of Na_2SiF_6 is a thermally activated process that can be adequately described by the shrinking core model, being SiF_4(g) and an ash layer of NaF(s) the dissociation products.
- Results from the ANOVA show that the parameter that most significantly impacts the fractional weight loss of Na_2SiF_6 is the processing temperature (with 51% percentage contribution), followed by the gas flow rate (24%), by processing time (15%), and finally the type of gas (3%).
- The optimal conditions to reach complete dissociation of Na_2SiF_6 are pure nitrogen as processing atmosphere, temperature of 650°C, processing time of 40 min, and gas flow rate of 100 cm^3/min. Maintaining all parameters and levels constant, using nitrogen, the fractional weight loss of Na_2SiF_6 is about 1.05–1.5 orders of magnitude greater than that in N_2:5% NH_3.
- While the decomposition temperature is not affected by the gas flow rate, it is influenced moderately by an increase in the heating rate.

- Within the NaF ash layer formed during Na_2SiF_6 decomposition, porosity decreases with increasing gas flow rate, time, and temperature.
- Applying the shrinking core model allowed establishing that regardless of atmosphere type, decomposition kinetics fits to a reaction order of $n \approx 0.12$ and that both chemical reaction and mass transfer mechanisms govern Na_2SiF_6 decomposition.
- The activation energy for Na_2SiF_6 dissociation in N_2 resulted to be lower than that in N_2:NH_3 at the same flow rates of 20, 60, and 100 cm^3/min. While in N_2:NH_3 the determined activation energies are 140, 120 and 115 kJ/mol, in N_2 the values are 121, 109, and 94 kJ/mol, correspondingly.

Niloofar Soltani and Amin Bahrami gratefully acknowledge CONACyT (Consejo Nacional de Ciencia y Tecnología, in Mexico) for granting a doctoral scholarship. Thanks also to Dr. Francisco Botello Rionda for technical assistance during the thermogravimetric analysis.

APPENDIX

The Taguchi experimental design, developed by Dr. Genichi provides a comprehensive understanding of the individual and combined effects of various design parameters based on a minimum number of experimental trials. The ANOVA method used in the Taguchi method is a statistical technique primarily adopted to evaluate the significance levels of control process parameters and the response of each parameter. In the ANOVA, many quantities such as degree of freedom (DOF), sum of squares, mean of squares, etc. are computed. These quantities and their interrelationships are defined below, and their mathematical development is presented.

CF = correction factor	n = number of trials	F = degree of freedom
E = error experimental	r = number of repetitions	S = sum of square
F = variance ratio	P = percent contribution	V = mean square (variance)

The sum of squares term can be defined as

$$S_T = \sum_{i=1}^{N} \left(Y_i - \bar{Y}\right)^2 \tag{A1}$$

which can be reduced by

$$S_T = \sum_{i=1}^{N} Y_i^2 - \frac{T^2}{N} \tag{A2}$$

The correction factor (CF) is used for calculation of all sums of squares. It remains constant for all factors as it composed of fixed quantities (T and N).

$$\mathrm{CF} = \frac{T^2}{N} \tag{A3}$$

The factor sum of squares is calculated by Eq. (A4)

$$S_A = \frac{A_1^2}{N_{A_1}} + \frac{A_2^2}{N_{A_2}} - (\mathrm{CF}) \tag{A4}$$

Mean squares (or variance) are simply the sum of squares per DOF, as

$$V_A = \frac{S_A}{f_A} \tag{A5}$$

The percent influence of the factors can now be calculated by comparing the pure sums of squares of the factors with respect to the total sum of squares, according to Eq. (A6)

$$P_A = \frac{S_A}{S_T} \tag{A6}$$

The percent influence of the error term is calculated by

$$P_e = 100 - (P_A + P_B + P_C) \tag{A7}$$

BIBLIOGRAPHY

1. Lyman, J. L.; Noda, T. J Phys Chem Ref Data 2001, 30, 165–186.
2. Wang, M.; Xie, M.; Ferraioli, L.; Yuan, Z.; Li, D.; Yang, D.; Pavesi, L. J Appl Phys 2008, 104, 083504.
3. Herrmann, M.; Klemm, H.; Schubert, C. Handb Ceram Hard Mater 2000, 749–801.
4. Tamura, A.; Inoue, K.; Onuma, T., Sato, M. Appl Phys Lett 1987, 51, 1503–1505.
5. Küppers, D.; Koenings, J.; Wilson, H. J Electrochem Soc 1987, 125, 1298–1302.
6. Johnson, G. J Chem Thermodyn 1986, 18, 801–802.
7. Rai-Choudhury, P. J Electrochem Soc 1971, 118, 266–269.
8. Padma, D.; Vasudeva Murthy, A. J Fluorine Chem 1974, 4, 241–242.

9. Padma, D. J Fluorine Chem 1974, 4, 441–443.
10. Padma, D.; Suresh, B.; Vasudevamurthy, A. J Fluorine Chem 1979, 14, 327–329.
11. Borisov, V.; Mel'nikova, S. Zh Prikl Khim 1984, 57, 705–707.
12. Bulanov, A.; Pryakhin, D.; Balabanov, V. Russ J Appl Chem 2003, 76, 1393–1395.
13. Kashiwaya, Y.; Cramb, A. W. Metall Mater Trans B 2002, 33, 129–136.
14. Vanka, M.; Vachuška, J. Thermochim Acta 1980, 36, 387–391.
15. Istomin, S.; Galkov, A.; Gul'din, I.; Kyun, A. Zh Prikl Khim 1979, 52, 2391.
16. Pech-Canul, M. I. BS thesis; Yucatan State University, Mérida, Mexico, 1988.
17. Leal-Cruz, A. L.; Pech-Canul, M. I. Solid State Ionics 2007, 177, 3529–3536.
18. Homma, S.; Ogata, S.; Koga, J.; Matsumoto, S. Chem Eng Sci 2005, 60, 4971–4980.
19. Levenspiel, O. Chemical Reaction Engineering; Wiley: New York, 1972.
20. Soltani, N.; Bahrami, A.; Pech-Canul, M. I.; González, L. A. Chem Eng J 2015, 264, 899–935.
21. Bahrami, A.; Pech-Canul, M. I.; Gutierrez, C. A.; Soltani, N. J Alloys Compd 2015, 644, 256–266.
22. Bahrami, A.; Pech-Canul, M. I.; Gutiérrez, C. A.; Soltani, N. Appl Surface Sci 2015, 357(Part A), 1104–1113.
23. Bahrami, A.; Soltani, N.; Pech-Canul, M. I.; Gutiérrez, C. A. Crit Rev Environ Sci Technol 2016, 46, 143–208.
24. Dundas, D.; Rost, J. M. Phys Rev A 2005, 71, 013421–8.
25. Pamuk, H. O. J Am Chem Soc 1976, 98, 7948–7950.
26. Sanchez, O.; Gomez-Aleixandre, C.; Fernandez, M.; Albella, J. M. Vacuum 1989, 39, 727–729.
27. Chang, C. P.; Flamm, D. L.; Ibbotson, D. E.; Mucha, J. A. J Appl Phys 1987, 62, 1406–1415.
28. Hagen, E.; Grande, T.; Einarsrud, M. A. J Am Ceram Soc 2004, 87, 1200–1204.
29. Kissinger, H. E. Anal Chem 1957, 29, 1702–1706.
30. Lu, H.-B.; Mazet, N.; Spinner, B. Chem Eng Sci 1996, 51, 3829–3845.
31. Gbor, P. K.; Jia, C. Q. Chem Eng Sci 2004, 59, 1979–1987.
32. Bishnoi, S.; Rochelle, G. T. Chem Eng Sci 2000, 55, 5531–5543.
33. Richardson, E. W. US Patent US3372004 A, 1968.
34. Stanmore, B.; Gilot, P. Fuel Process Technol 2005, 86, 1707–1743.
35. Richerson, D. Modern Ceramic Engineering: Properties, Processing, and Use in Design; CRC Press: Boca Raton, FL, 2005.
36. Geiger, G. H.; Poirier, D. R. Transport Phenomena in Metallurgy. Addison-Wesley, Reading, MA, 1973.
37. British Standard Institution, BS 4359 Part 2, 1982.
38. Hongo, M.; Iwasaki, H. Rev Phys Chem Japan 1977, 47, 90–101.